

Crater Detection using CGC

A New Circle Detection Method

Vinciane Lacroix¹ and Sabine Vanhuyse²

¹CISS Department, Royal Military Academy, Brussels, Belgium

²IGEAT, Université Libre de Bruxelles, Brussels, Belgium

Keywords: Circle Detection, Crater Detection, Constrained Gradient, Feature Extraction.

Abstract: "Constrained Gradient for Circle" (CGC) is a new circle detection algorithm based on the gradient of the intensity image. The method relies on two conditions. The "gradient angle compatibility condition" constrains the gradient of a given percentage of the pixels belonging to some digital circles having a radius in the range of radii to detect to point towards the centre of the circle or in the opposite direction. The "curvature compatibility condition" constrains the variation of the gradient angle of the same pixels in a range depending on the radius of the circle. These two conditions are sufficient to detect the core of circular shapes. The best-fitting circle is then identified. The method is applied to artificial and reference images and compared to state-of-the-art methods. It is also applied to water-filled crater detection in Cambodia: these craters that might indicate the presence of Unexploded Ordnance (UXO) dating from the US bombing produce dark circles on satellite panchromatic images.

1 INTRODUCTION

The presence of Unexploded Ordnance (UXO) resulting from the US bombing during the late 1960s and 1970s is still preventing the use of the land in Cambodia. When dropped, the bombs produced craters that may still exist today. Many of them are filled with water so that they appear as circular objects on panchromatic satellite images. The purpose of this study is to extract those craters as they might indicate the presence of UXOs. Similar work was made by Hatfield Consultants (Hatfield-Consultants, 2014) for Laos. The authors used historic Corona satellite images; they computed differences between the original image and its smoothed version, and used these differences in an unsupervised K-means fuzzy classifier. One class contained the impacted areas which were then identified based on geometrical characteristics. The geometry (i.e. the fact that craters are almost circles) is being used at the end of the process whereas our approach is rather to start with geometry, i.e. dark circle detection.

Circle detection has been a challenge since the early days of Pattern Recognition and is still arousing interest as recent publications show ((Chung et al., 2012), (Akinlar and Topal, 2013), (Marco et al., 2014)). Exhaustive review of circle detection meth-

ods can be found in the introduction of these articles. "Circle" may designate the border of a "sphere", "disc" or "ring", or, a very thin ring, as shown on Figure 1. In this publication, we are interested in "disc" detection, although the proposed method can be used as such for sphere detection and for detecting inner ring circumference. The method may be adapted for the detection of the other types of circles but such an adaptation is not described here.

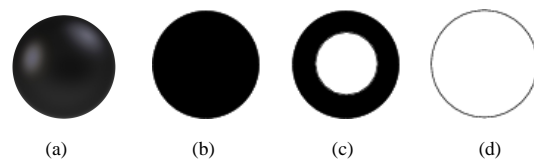


Figure 1: (a) Sphere; (b) disc; (c) ring; (d) thin ring.

Hough transforms and their randomised versions are very popular (see for example (Xu et al., 1990), (Yip et al., 1992)) but are still very time consuming as they rely only on the hypothesis of three edgels belonging to a circle and they may require complex structures for storing the votes. Some computational time may however be saved using the gradient orientation to constrain edgels belonging to the same circle (see for example (Atherton and Kerbyson, 1999)) or using a LUT method ((Chung et al., 2009)).

Most existing approaches use the fact that some basic elements (pixels, edgels, or connected segments) are part of the circumference and combine some of them to generate a centre-radius pair hypothesis. To our knowledge, none of them uses a “blind” centre-radius hypothesis as detecting circles of various radii at each pixel seems time-consuming.

However, performing a first test on the *gradient angle* on a few pre-defined digital circles of radius spanning the radius range to detect allows to isolate the core of shapes (circle, ellipses, squares, etc.) of the corresponding size. This test requires the gradient angle of pixels located on the digital circles to be *similar* to the angle of the line joining the pixel to the circle centre. The second test consists in checking if the *gradient angle variation* of pixels located on the same circle are compatible with the one associated with the considered circle. The second test enables to keep circular shapes only. A counter is set at each pixel considered as a potential centre and is incremented if both tests are positive for the considered digital circle. The percentage of compatible pixels is stored and if the counter represents a significant part of the digital circle, the centre is considered as a potential candidate.

A second phase is however necessary to identify the best centre/radius pair among the candidates. In order to ease the second phase, in this publication, we assume that the circles present in the image do not overlap, and thus, if there is a circle at some pixel, it is unique. This assumption is valid for the crater detection application we are concerned with but might not be true for other applications.

As the method is based on constrains on the gradient, it is called “CGC” meaning “Constrained Gradient for Circle”.

This paper is organized as follows. Section 2 presents the first phase aiming at extracting centres candidates. In that section, the gradient angle and the curvature compatibility conditions are presented. The algorithm is then described and applied to an artificial image. In Section 3, a second phase aimed at extracting the best centre-candidate and the adequate circle is proposed. In Section 4 the results of the full process applied to three different images are presented and compared to the ones of state-of-the-art methods. Discussion and conclusions are provided in Section 5.

2 EXTRACTING CENTRES CANDIDATES

In natural images or in scanned graphics, pure step edges are not very probable; edges are rather span-

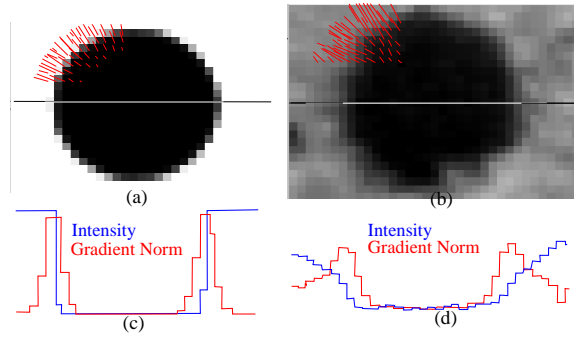


Figure 2: (a) Scanned graphic and (b) natural image with some scaled gradient vectors overlaid and in (c-d) their respective Intensity (in blue) and gradient norm profiles (in red) at the centre line.

ning over a few pixels, which makes hills of gradient norm even broader; in this study we use the Gaussian gradient (Canny, 1986) with $\sigma = 1$. In the vicinity of the border of a circle, the gradient orientation is near the line passing through the centre, although the discretization process makes it dependent on the angle and position (see Figure 2). Moreover, the variation of the gradient angle in the direction perpendicular to the gradient depends on the distance of the pixel to the centre. These properties are exploited in the first phase of the process.

2.1 Compatibility Conditions

2.1.1 Gradient Angle

In order to have a circle of radius r at centre c , all gradient vectors located on the digital version of the circle should point either towards c (bright circle) or in the opposite direction (dark circle); because of the discretization process, they will not point *exactly* along this direction, but the angle difference should be small (see the examples of Figure 2).

Let angles be expressed in fraction of radian (i.e. unit= radian/ π) so that the angle range is $[-1 1]$. Let p be a pixel located on a digital circle C of radius r at centre c , let γ be the gradient angle at p , and let α be the angle of the line joining p to c . If there exists a circle of radius r at c , the **gradient angle compatibility condition at c** is defined as: $\forall p \in C$,

$$\begin{aligned} \text{Diff}(\alpha - \gamma) &< \varepsilon_a && \text{for dark circle} \\ \text{Diff}(\alpha - (1 - \gamma)) &< \varepsilon_a && \text{for bright circle} \end{aligned} \quad (1)$$

where Diff denotes angle difference.

This condition is necessary but not sufficient: it is also true for “centres” of other shapes such as circles of radius r' close to r (depending on the edge profile

and on the extent of the filter in the gradient computation), for ellipses of axis close to r , and for shapes fitting in circles of similar radius values. Moreover, depending on the tolerance on the angle difference ϵ_a , the condition in (1) will not only hold for the centre of the shape but also for its neighbourhood.

2.1.2 Gradient Angle Variation

If p is located on a digital circle, the local variation of the angle of the gradient is also constrained. Let s and t the two points located at a distance δ in the direction perpendicular to the gradient at p . Let κ be defined according to the Equation 2.

$$\kappa = \text{Diff}(\gamma_s - \gamma_t) \tag{2}$$

where γ_s and γ_t denote the gradient angle at s and t . κ is an approximation of the local curvature at p and will abusively called ‘‘curvature’’ in the following. If r is the radius of the circle, κ is such that

$$\kappa = 2 * \arcsin(\delta/r) \tag{3}$$

Some tolerance on the curvature should also be allowed to deal with the discretization process. Thus the **curvature compatibility condition at c** is defined as: $\forall p \in C$,

$$\begin{aligned} 2 * \arcsin(\delta/r) - \epsilon_k < \kappa_p < 2 * \arcsin(\delta/r) + \epsilon_k \\ \kappa_r - \epsilon_k < \kappa_p < \kappa_r + \epsilon_k \end{aligned} \tag{4}$$

where ϵ_k designates the tolerance on the curvature and κ_p the curvature at p .

Figure 3 illustrates the two constraints for a pixel p located at angle α on the circle C of radius $r = 6$.

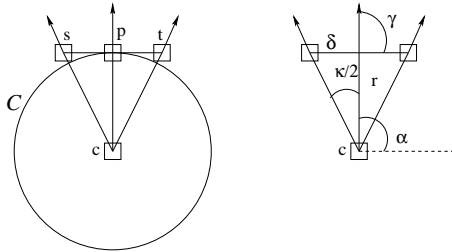


Figure 3: Constraint on gradient angle γ and on curvature κ at p located on circle C of radius r ; s and t are located at a distance δ of p in the direction perpendicular to γ .

In the case of an imperfect or partial circle of radius r , only a fraction f of the gradient angles located on C will satisfy condition (1) and (4). The number of pixels n that should satisfy the angle and the curvature compatibility condition, and b , the maximum number of non-valid pixels are thus defined by

$$n = f \# C \text{ and } b = (1 - f) \# C \tag{5}$$

where $\#$ denotes the cardinality.

If the circles to detect have a radius between r_{min} and r_{max} , thanks to the smooth variation of the gradient direction in the direction perpendicular to the border (see Figure 2), not all corresponding digital circles need to be tested for angle and curvature compatibility. In this publication we use all integer values of r between r_{min} and r_{max} by step of two.

There exist several implementations of digital circles (Blinn, 1996). In this study, the pixels of the digital circle C of radius r are found by starting at pixel $p(i, j) = (0, r)$, incrementing i by one, computing j using the circle equation, and computing the angle using arcsin until $0.25 (\pi/8)$ is reached; the other pixels are found using the circle symmetries (see some resulting circles in Figure 4). The chosen implementation — also known as Bresenham’s circle algorithm — is the one that has the smallest number of pixels while preserving the connectivity.

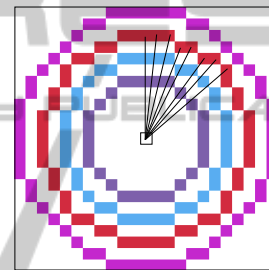


Figure 4: Digital circles used in this study for a radius range from 5 to 12 and a few vectors joining the centre to the pixels lying on the circle of radius $r = 9$; each digital circle is displayed in a different color.

2.2 Phase One: Algorithm Description

2.2.1 Prerequisite

1. Compute Gaussian gradient G_x, G_y and norm N .
2. Compute Angle of gradient A , and curvature K according to Equation 2.

2.2.2 Centre Candidates

Let $\epsilon_a, \epsilon_k, f$ and t be the tolerance on gradient angle, the tolerance on curvature, the fraction of circle to detect and the threshold value under which the norm of gradient is considered as noise respectively.

1. Let $C = \{C_0, \dots, C_j, \dots, C_n\}$ be the list of digital circles located at the origin, corresponding to the increasing radii $r_0, \dots, r_j, \dots, r_n$ with $r_{min} = r_0$ and $r_n \leq r_{max}$. For each C_i , get the list of vectors p_{ij} joining the centre to each pixel located on the digital circle (i.e. using Bresenham’s algorithm) and their angle a_{ij} ; compute $z_i = \# C_i, b_i$ and n_i ac-

cording to Equation 5 and the ideal curvature κ_i according to Equation 3.

2. Initialize two rasters R and V for storing the radius and the fraction of valid pixels.
3. Scan the image; for each pixel c , compute the fraction of valid pixels lying on the digital circles $\{C_0, \dots, C_j, \dots, C_n\}$ starting with the smallest circle C_0 , as follows. For each vector p_{ij} of C_i , get the pixel $q_{ij} = c + p_{ij}$, lying on circle C_i centred at c and test three conditions:
 - the minimum norm condition: $N_{q_{ij}} > t$;
 - the angle difference compatibility condition according to Equation 1, where $\alpha = a_{ij}$ (angle of p_{ij}) and $\gamma = A_{q_{ij}}$ (gradient angle at q_{ij});
 - the curvature compatibility condition according to Equation 4 where κ is the curvature at q_{ij} and $\kappa_r = \kappa_i$.

If all conditions are satisfied, increment the “good” counter at c (count separately dark and bright circle according to the gradient angle at q_{ij}), otherwise increment the “bad counter”. As soon as the bad counter has reached b_i , the next circle C_{i+1} is tested. Otherwise, test the full circle C_i , save r (radius) and v (fraction of valid pixel) in R and V respectively. For convenience purpose, a negative value in V indicates a dark circle. Store c in a list of potential centre candidates.

2.2.3 Shapes’ Core

Get the connected components of all centre candidates. In the case of non-overlapping circles, each connected component will be the core of a circular shape. For each connected components, compute c_a , the centre of gravity of the pixels with the lowest radius r (it should be a centre candidate, but if it is not, consider the 8-neighbours of similar radius with the highest counter). $c_a - r$ is a first centre-radius approximation of the shape.

2.3 Application

The parameters of the proposed method are:

- $\sigma = 1$ and $\delta = 2$ for the prerequisite Gaussian gradient and curvature computation,
- $t = 10$ for ignoring pixels with a too low gradient norm,
- ϵ_a, ϵ_k , for setting the tolerance on gradient angle and curvature; expressed in fraction of radian (i.e. unit= radian/ π), a reasonable range is $[0.06 \ 0.14]$. For simplicity $\epsilon_a = \epsilon_k$.

- f , for the minimal fraction of circle to detect. A reasonable range is $[0.7 \ 1]$;

The fraction of detected circle v at some potential centre depends on ϵ_a/ϵ_k : if the tolerance rises, the portion of detected circle will stay equal or become larger. The parameters f and ϵ_a/ϵ_k are thus not independent.

Experiments on geometric figures on a uniform background provide some insight on the method (used with $rmin = 5$ and $rmax = 15$) and enable to analyse the effect of the parameters ϵ_a, ϵ_k , and f on the production of candidates. The shapes are identified by numbers on Figure 5 (top). The raster V displaying v , the fraction of the smallest valid circle at each centre candidate, has been analysed for values of $\epsilon = \epsilon_a = \epsilon_k$, ranging from 0.06 to 0.14, and $f = 0.6$. Although 0.6 is below the recommended value, it enables to see when false alarms occur for low f values. An example of such a raster is shown on Figure 5 (bottom) for $\epsilon_a = \epsilon_k = 0.12$ and $f = 0.6$. Connected sets of non-zero v values correspond to the core of each shape, except for the ellipse (26) which generates two connected sets when $\epsilon = 0.14$. The minimum and maximum values of v in the core of each shape are shown in Table 1. None of the triangle generates a connected component; they are thus ignored in the table; they are nevertheless important in the experiment as their proximity to near-circular shapes is disturbing their detection by perturbing the gradient direction (see shapes 9–10, 13–14, 23–24).

Table 1: Percentage range of compatible pixels for the core of each shape identified in Figure 5.

Type ↓	$\epsilon \rightarrow$ Id ↓	0.06	0.08	0.10	0.12	0.14
Circle	14					
	15					
Circular Ellipse	10	60-100	63-100	77-100	60-100	60-100
	11		65-95	60-100	61-100	60-100
	18	60-98	60-100	60-100	60-100	60-100
	23	60-85	61-95	63-100	63-100	60-100
Elipse	1	60-70	60-85	60-96	60-100	60-100
	4	61-85	60-69	60-88	60-95	60-100
	12		90	71-85	60-92	60-92
	26	60-70	60-90	60-95	60-95	60-100
Square	2					60
	3				66	61
	5				60	60-84
	6					60-63
	7					60-67
	17				60	61-71
	19					60-63
	21					61
	29					65-84
						61-63

The image contains two perfect circles (14, 15), four almost circular ellipses (10, 11, 18, 23), other ellipses (1, 4, 12, 26) and squares (2, 3, 5, 6, 7, 17, 19, 21, 29). The analysis of the table suggests using the method with $\epsilon \simeq 0.12$, as for any value of $f > 66$, all circles and almost circular ellipses will be detected, and so will be the ellipses (1, 4, 12). A higher value of ϵ might generate false alarms among squares, al-

though setting $\epsilon_k < \epsilon_a$ might resolve them. A smaller value of ϵ might be inadequate to deal with practical problems more subject to noise.

The same image has been processed using the isophote (Marco et al., 2014) and the EDCircles (Akinlar and Topal, 2013) method (see Figure6). The sets of detected shapes are slightly different:

- CGC: ($\epsilon = 0.12, f > 66$): {14, 15, 10, 11, 18, 23, 1, 4, 12};
- Isophote: {14, 15, 10, 11, 18, 1, 12};
- EDCircles: {14, 15, 10, 11, 18, 1, 4, 12, 26};

All methods detect the perfect circles (14,15); Isophote and EDCircles are missing the near circular ellipse 23 probably because of the proximity of shape 24. Some ellipses are detected by all methods; Isophote rejects the most elongated ones. None of the methods generate false alarms.

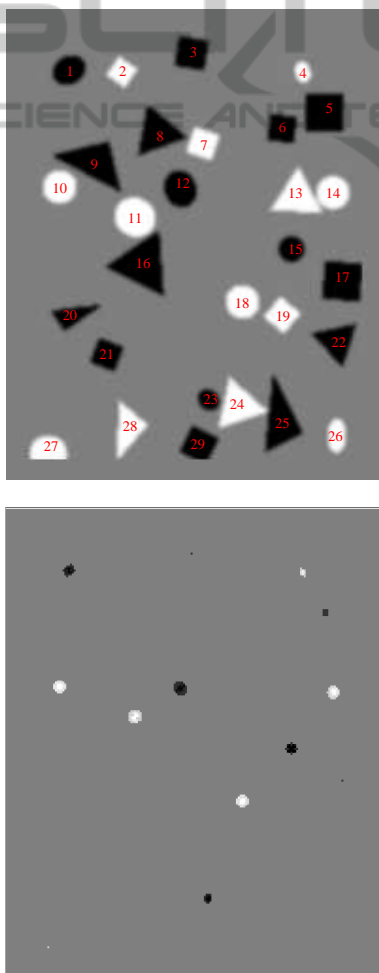


Figure 5: (Top) Test image made of random geometrical dark and bright shapes; (bottom) Example of Raster V ($\epsilon_a = \epsilon_k = 0.12$ and $f = 0.6$); white= 100% detection for bright circle, grey=0% , black= 100% detection for dark circle.

3 BEST CENTRE-CIRCLE CANDIDATES

The first phase enables to detect the core of each circular shape; the second phase aims at finding the best centre-radius pair. A first centre approximation (c_a) is obtained selecting the centre of gravity of pixels of the lowest radius value inside the connected component. The exact centre should be in the vicinity of this point, and provided that there is a unique circle near c_a (working hypothesis), the exact radius should be in the range of $[r \ r + 2]$.

One could use any existing circle detection method in the neighbourhood of c_a , or use active contours with the circle of radius r_{min} as initial contour or consider the estimation of the parameter of the potential circles in these areas as a least square estimation problem such as in (Zelniker, 2006).

The problem thus becomes an optimization problem: find the best circle given a centre and find the best centre within the set associated with the same label. The best optimization function will depend on the application: e.g., is a partial circle that fits the border of the shape perfectly a better output than a complete circle lying farther away from this border? Different choices will lead to different optimization functions.

Nevertheless, three factors are important in the process: the gradient angle and curvature compatibility as already identified in the first phase, and also the location of the shape border that depends on the gradient norm, the latter being maximum at edgels.

The current implementation of the second phase is described as follows. For each shape label, each digital circle of radius in the range of r to $r + 2$ at centre c_a (identified by phase one) is tested as the potential circle. For each of these circles, pixels satisfying the three compatibility conditions (norm, angle and curvature) are considered: the projection of the gradient along the line joining the pixel to the centre is computed and the average n_a is performed on the circle. The fraction of valid pixel v is computed. The circle with the highest value of $n_a * v$ is considered as the best fit. The second phase is thus very similar to the the first one, excepted that:

- more precise circles are used (r incremented by one),
- only centre of gravity of shapes are tested
- an additional computation involving the gradient is performed at each pixel

An integer value is thus obtained for the centre and for the radius.

4 RESULTS

The full detection method has been applied to an artificial image, to a reference image and to a satellite image; the results are compared to the results obtained by the using the isophote (Marco et al., 2014) and the EDCircles (Akinlar and Topal, 2013) method.

4.1 Application to an Artificial Image

The results of phase one on the image displayed in Figure 5 has already been described and discussed in Section 2.3. The method is used with $\sigma = 1$ and $\delta = 2$ for the norm and curvature computation, $\epsilon_a = \epsilon_k = 0.12$, $t = 10$, $f = 0.80$, $rmin = 5$, $rmax = 15$. The best-fitting circles are shown on Figure 6.

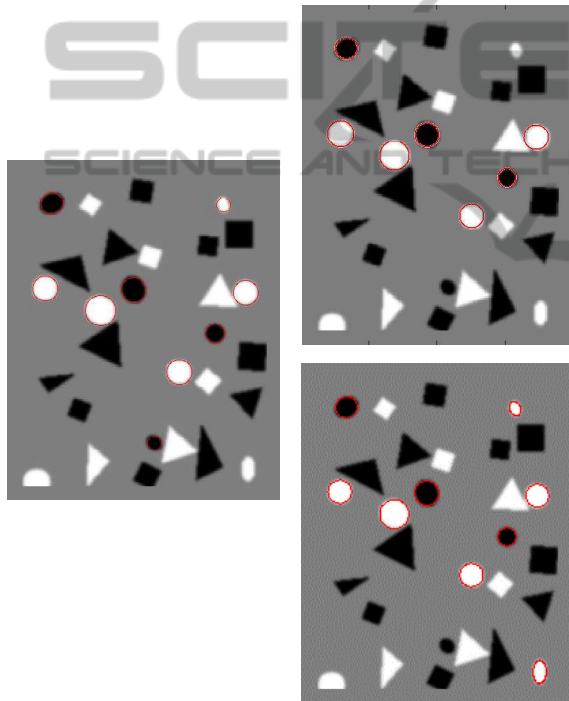


Figure 6: Detected circles superimposed on Test image made of random geometrical dark and bright shapes (200×250); left: CGC; top right: isophote; bottom right: EDCircle.

4.2 Application to a Reference Image

The CGC method with the same parameter values (except for $rmax$ set to 50) has been used to detect circular shapes on the image shown in Figure 7 available at

<http://ceng.anadolu.edu.tr/cv/EDCircles/>

where the result of the EDCircle method is also compared to other methods.

Note that the wheels of the car on the right sign

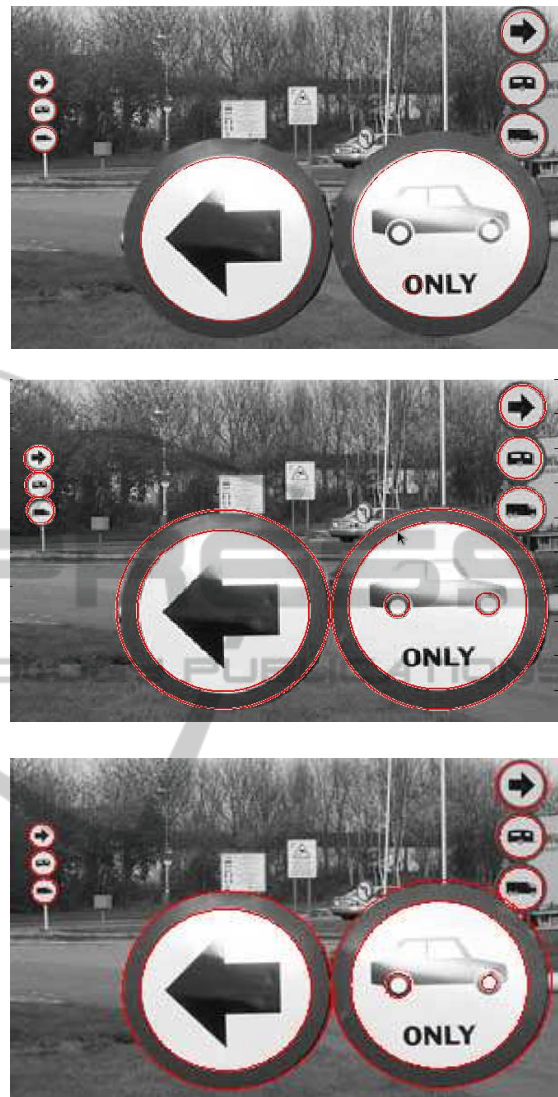


Figure 7: Detected circles superimposed on Sign Image (300×198); (top) CGC (middle) Isophote; (bottom) EDCircle.

are detected by the Isophote and EDCircle methods. The white discs inside the wheels are too small for the CGC (although it is recommended to use the CGC with $rmin \geq 5$, if $rmin$ is set to 4, the disc of the left wheel is detected). The outside circles of the two big signs are missed by the CGC, as a single circle is assumed at a given location. Only the CGC is detecting the "O" of "only"; even the EDCircle is missing it although it detected shape 26 of Figure 5. Thus, with respect to sign detection the CGC performs as well as the best state-of-the-art methods.

4.3 Application to a Satellite Image

The study area is located in the eastern part of

Cambodia near the border with Vietnam, in a rural zone (Choam Kravien) that was heavily bombed during the Vietnam War. The terrain is quite flat and the landscape consists mainly of agricultural land. The panchromatic image used was acquired by the WorldView-2 instrument on 26 November 2011. It covers 100 km², with a spatial resolution of 0.5 meter and a pixel depth at acquisition of 11 bits. The method is used with $\sigma = 1$ and $\delta = 2$ for the norm and curvature computation, $\epsilon_a = \epsilon_k = 0.12$, $t = 10$, $f = 0.80$, $r_{min} = 5$, $r_{max} = 15$; only dark circles are detected and an additional threshold on the circle average norm n_a is set at $t = 50$.

The results using our method, isophote and ED-Circles are respectively shown in Figure 8, 9 and 10.

The comparison of the results shows that many circle shapes are missed by the EDCircle; many are detected by the isophote method but the CGC method provide better results. A comparison with visual inspection should still be performed to have a quantitative view of the performance of the method in this context.

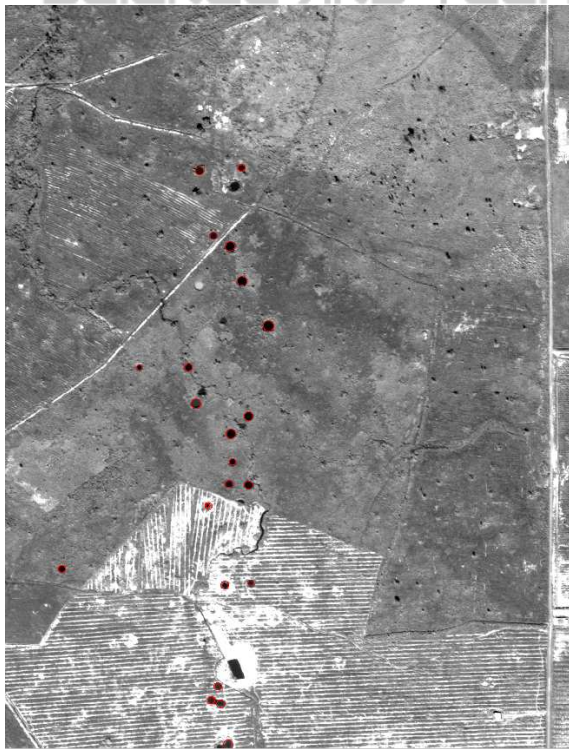


Figure 8: Detected circles (CGC) superimposed on 1309×1855 part of the panchromatic image.

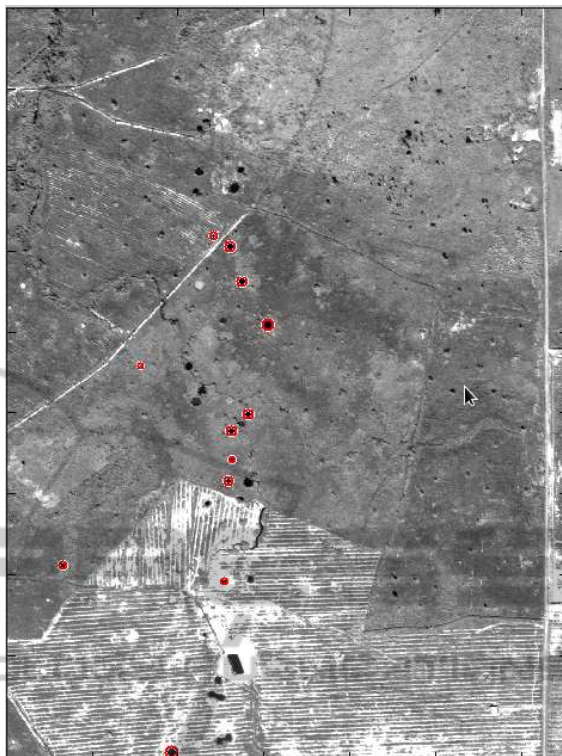


Figure 9: Detected circles (Isophote method) superimposed on 1309×1855 part of the panchromatic image.

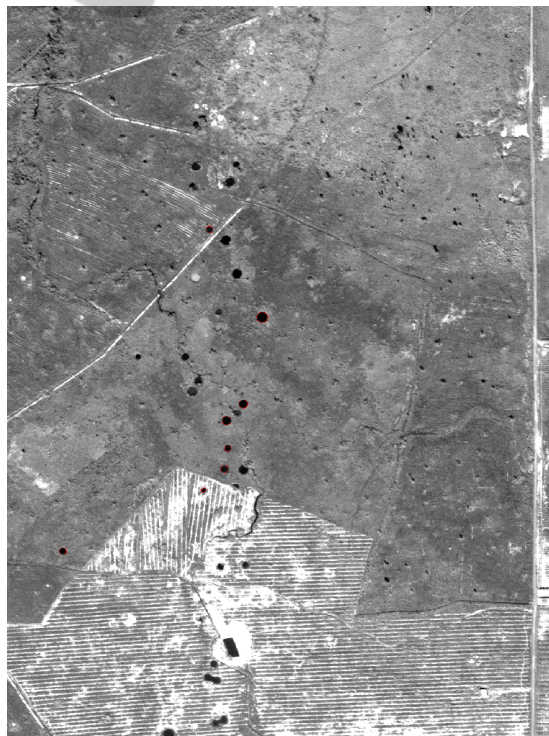


Figure 10: Detected circles (EDCircle method) superimposed on 1309×1855 part of the panchromatic image.

5 DISCUSSION AND CONCLUSIONS

The Constrained Gradient for Circle (CGC), a new two-phase method for extracting circles seems promising. The originality of the method resides in the first phase that uses a gradient angle and curvature compatibility constraint at pixels lying on various digital circles to produce sets of connected pixels belonging to potential circle candidates. The second phase consists in finding the best pair of circle-centre that optimizes the circle position. The method has been compared to state-of-the-art methods applied to an artificial image, a reference image and a panchromatic satellite image of Cambodia for crater detection. The results seem promising. The process could be performed in parallel, not only at each pixel, but also for each of the digital circles, which makes the method efficient. Although the method in the current form can deal with any radius range and various portions of circle, it is better suited to the detection of full disconnected circles whose radius is small compared to the image size. It could be generalized in order to extract overlapping circles, rings and thin rings by developing another second phase (thin ring detection would require a further line detection step as prerequisite) and also to detect squares, by adapting the curvature compatibility constraint.

ACKNOWLEDGEMENTS

Special thanks to Dr. De Marco who processed our data with his method, and to Dr. Akinlar and Dr. Topal for their site at

<http://ceng.anadolu.edu.tr/cv/EDCircles/except>

which allows to process any data with their method. This research is funded by the EC FP7 Security TIRAMISU Project GA 284747.

REFERENCES

- Akinlar, C. and Topal, C. (2013). Edcircles: A real-time circle detector with a false detection control. *Pattern Recognition*, 46.
- Atherton, T. J. and Kerbyson, D. J. (1999). Size invariant circle detection. *Image and Vision Computing*, 17:795803.
- Blinn, J. (1996). *Jim Blinn's Corner: A Trip Down the Graphics Pipeline*. Morgan Kaufmann series in computer graphics and geometric modeling. Morgan Kaufmann Publishers.
- Canny, J. (1986). A computational approach to edge detection. *IEEE Trans. on Pattern Anal. and Machine Intelligence*, pages 679–697.
- Chung, K.-L., Chen, P.-Z., and Pan, Y.-L. (2009). Speed up of the edge-based inverse halftoning algorithm using a finite state machine model approach. *Computers & Mathematics with Applications*, 58(3):484 – 497.
- Chung, K.-L., Huang, Y.-H., Shen, S.-M., Krylov, A. S., Yurin, D. V., and Semeikina, E. V. (2012). Efficient sampling strategy and refinement strategy for randomized circle detection. *Pattern Recognition*, pages 252–263.
- Hatfield-Consultants (2014). Uxo predictive modeling in mmg lxml sepon mine development area. Technical Report 1791.D6.1, Hatfield consultants, East Lansing, Michigan.
- Marco, T. D., Cazzato, D., Leo, M., and Distanto, C. (2014). Randomized circle detection with isophotes curvature analysis. *Pattern Recognition*.
- Xu, L., Oja, E., and Kultanen, P. (1990). A new curve detection method: Randomized hough transform (rht). *Pattern Recognition Letters*, 11:331338.
- Yip, R. K., Tam, P. K., and Leung, D. N. (1992). Modification of hough transform for circles and ellipses detection using a 2-dimensional array. *Pattern Recognition*, 25:10071022.
- Zelniker, E. E. (2006). Maximum-likelihood estimation of circle parameters via convolution. *IEEE Transaction on Image Processing*, 16:865–876.